ADVANCED OPTICAL MATERIALS
www.advopticalmat.de

Superradiance Emission and Its Thermal Decoherence in Lead Halide Perovskites Superlattices

Hamid Pashaei Adl, Setatira Gorji, Guillermo Muñoz-Matutano, Andrés F. Gualdrón-Reyes, Isaac Suárez, Vladimir S. Chirvony, Iván Mora-Seró, and Juan P. Martínez-Pastor**

Self-assembled nanocrystals (NCs) into superlattices (SLs) are alternative materials to polycrystalline films and single crystals, which can behave very differently from their constituents, especially when they interact coherently with each other. This work concentrates on the Superradiance (SR) emission observed in SLs formed by $CsPbBr_3$ and $CsPbBrI_2$ NCs. Micro-Photoluminescence spectra and transients in the temperature range 4–100 K are measured in SLs to extract information about the SR states and uncoupled domains of NCs. For $CsPbBr_3$ SLs with mostly homogeneous SR lines (linewidth 1–5 meV), this work measures lifetimes as short as 160 ps, 10 times lower than the value measured in a thin film made with the same NCs, which is due to domains of near identical NCs formed by 1000 to 40 000 NCs coupled by dipole–dipole interaction. The thermal decoherence of the SR exciton state is evident above 25 K due to its coupling with an effective phonon energy of ≈8 meV. These findings are an important step toward understanding the SR emission enhancement factor and the thermal dephasing process in perovskite SLs.

1. Introduction

Coherent spontaneous emission is a fundamentally interesting topic in quantum optics. It has received a lot of attention since Dicke's seminal work.[1] Dicke predicted the cooperative emission from a dense excited two-level system of gaseous atoms or molecules in the absence of a laser cavity in 1954,[1] and shortly after, Bonifacio and Lugiato classified it into two distinct forms:[2] Dicke Superradiance (SR) and Superfluorescence (SF). When a system of N atoms interacts ($N \gg 1$), a typical many-body phenomena known as "Cooperative emission" arises, and the intensity of the emission is proportional to N^2 at the limit of $T = 0$ K. SR is a typical case of cooperative emission from a "correlated" state with an extended electric dipole.[2] The SR is then caused by an extended dipole's emission, and the phenomenon can be described in purely classical terms. SR has been reported in a variety of structures and systems, particularly aggregates and crystals of conjugated organic molecules,[3] diamond nitrogen vacancy centers,[4] and epitaxial quantum dots.[5,6] J-aggregates[7–13] are molecular aggregates with a narrow absorption line that is shifted[3] to a longer wavelength in comparison to the monomer absorption line and a narrow nearly resonant fluorescence line. These systems are very attractive, as it can be understood as a kind of mirrorless laser,[14] fully operated with a phase matched macroscopic mode.

For the sake of manipulation, control and scalability, it is very important the development of such photon sources by means of mesoscopic emitters, and hence artificial quantum nanostructures represent very promising alternatives under recent

H. Pashaei Adl, S. Gorji, G. Muñoz-Matutano, I. Suárez, V. S. Chirvony, J. P. Martínez-Pastor
Instituto de Ciencia de Materiales (ICMUV)
Universidad de Valencia
C/Catedrático José Beltrán, 2, Paterna E-46980, Spain
E-mail: hamid.pashaeiadl@uv.es; juan.mtnez.pastor@uv.es

The ORCID identification number(s) for the author(s) of this article can be found under https://doi.org/10.1002/adom.202202497

DOI: 10.1002/adom.202202497

I. Suárez
Departamento de Ingeniería Electrónica
Escuela Técnica Superior de Ingeniería
Universidad de Valencia
Avenida de la Universidad s/n, Burjassot 46100, Spain

A. F. Gualdrón-Reyes, I. Mora-Seró
Institute of Advanced Materials (INAM)
Universitat Jaume I
Avenida de Vicent Sos Baynat, s/n, Castelló de la Plana 12071, Spain

A. F. Gualdrón-Reyes
Facultad de Ciencias Instituto de Ciencias Qumicas
Isla Teja
Universidad Austral de Chile
Valdivia 5090000, Chile

analysis. Lead halide perovskites are highly efficient optoelectronic materials, with high optical absorption coefficient, which are considered as great low-cost alternatives for high efficient photovoltaic devices.[15] Nowadays, perovskite Nanocrystals (NCs) with usual cubic shape, are receiving a lot of attention in the field of LEDs[16] and displays,[17] due to the very narrow emission at room temperature, limited by the homogeneous linewidth of single NCs.[18–20] One of nature's most powerful tools for developing innovative functional materials is self-organization, which minimizes the need of complex procedures for manipulating individual building blocks. Controlled evaporation of the solvent at room temperature can be used to self-assemble cubic perovskite NCs on hydrophobic glass substrates, forming cuboidal superlattices (SLs). The transformation from disordered NCs dispersed in liquid to an ordered SL is set to continue during the drying stage. Due to the electrical and magnetic interactions between the NCs, these superstructures have shown SR emission (in some cases also SF),[21–30] which is identified by its bright, red-shifted emission compared to non-correlated emission from NCs in suspension or standard films prepared by spin-coating or other solution processing methods. Although the origin of this red-shifted emission from SLs still is under debate,[29–35] these works open the door to the manipulation and control of a large number of coherent photon bundles or bursts. However, up to date, the SR emission from perovskites SLs have been limited to cryogenic temperatures,[21,22,26,28,36–38] which represents an important obstacle to develop any practical device performance for future applications. To this concern it is also crucial the study and analysis of the temperature decoherence processes affecting the emission of 3D perovskite SLs.

In the present work we have investigated the optical emission of self-assembled SLs of cubic-shaped $CsPbBr_3$ and $CsPbBrI_2$ NCs forming cuboidal/parallelepiped SLs with edge sizes of several microns. In the case of SLs made of high quality (relatively low size dispersion) and sufficiently large NCs (>8 nm), we were able to measure by means of micro-photoluminescence (μ-PL) very narrow SR emission lines (1–5 meV) characterized by an enhancement factor up to ≈10, which is probed by the strong reduction of their lifetime with respect to standard films of NCs and also by their intensity in comparison to background emission of uncoupled NCs. We associate these SR lines to ordered subdomains with NCs of similar size inside the laser excitation volume (≈10^6 NCs) of the micrometric SLs (5×10^8 NCs), which are formed by 1000 to 40 000 NCs coupled by dipole-dipole interaction. SR emission was also investigated in SLs formed by smaller NCs (<7 nm) and mixed anion $CsPbBrI_2$ NCs, with broader lines and smaller enhancement factors, due to the effect of larger inhomogeneities in the assemblies promoted by simultaneous changes in edge size, and compositional fluctuations at every NC in the case of alloyed NCs. Thermal decoherence of SR was analyzed with spectral and transient μ-PL measurements as a function of temperature, resulting in a low activation energy within the radiative emission range (0–100 K), which can be associated with the dephasing of the SR exciton state by the coupling with low energy phonons (possibly an average between optical and folded acoustic ones). The quenching of the SR state observed above 25 K is translated into an increase in the population of localized excitons at higher energy NC states (mostly uncoupled); Above 70–80 K the exciton recombination dynamics in SLs begins to be similar to that observed in thin films, with an average lifetime increasing with temperature (>2 ns) and dominated by the trapping-detrapping dynamics of carriers in shallow levels.[39] The analysis of intrinsic and extrinsic factors related to SR decoherence is a key point for future designs in advanced optoelectronic applications, such as the engineering of NOON quantum states[40] or N photon bundles,[41] which have been recent areas of study for the development of novel light-based quantum technologies.[42]

2. Results

We synthesized colloidal NCs of cesium LHPs ($CsPbBr_3$, $CsPbBrI_2$), which can be prepared with a low dispersion of size and are characterized by their weak quantum confinement effects, which contribute to narrow-band emission at room temperature (see our previous work on $CsPbBr_3$ single NCs[19]). SLs of NCs are formed by solvent drying-induced spontaneous assembly,[32,43–45] (see Experimental Section). Individual cuboidal SLs are formed during the self-assembly process, each containing ≈10^8 NCs whose morphology can be nicely observed under the optical microscope (**Figure 1**a). These $CsPbBr_3$ NCs have an average size of ≈6–7 nm (see Figure S1, Supporting Information, for PL-PLE spectra of these NCs in solution at room temperature and PL spectra for different temperatures measured in a film). The estimation of the SL height was made by using a mechanical profilometer, after the metallization of the SL sample by depositing a 10 nm thick gold layer using thermal evaporation (see the aspect at the optical microscope in the image of Figure 1b), in order to minimize the contamination of the profilometer tip with the organic ligands. The histograms for lateral size and height measured in these SLs after preparation are shown in Figure 1c,d, respectively. According to these histograms, we obtain that the average lateral size of SLs is ≈10 μm and their corresponding average height ≈2.4 μm, hence the SLs grow as square parallelepipeds with an aspect ratio ≈0.25 (i.e., four times smaller in the vertical direction).

We also measured type A SL samples by θ–2θ X-Ray Diffraction in comparison to a film prepared by dipping into the same concentrated solution used for the fabrication of the SL, as summarized in Figure S2, Supporting Information. In the film we appreciate very well the peak at $\approx 2\theta = 30.5°$, which is a clear signature of the $CsPbB_3$ material (cubic or with tetragonal/orthorhombic deformation) and some contributions at ≈15° and 21–22°. In the case of SLs, we clearly observe a preferential orientation of the nanocubes, because only observed diffractions of (001), in the region of 2θ ≈15°, and (002) at $2\theta = 30.5°$. In the two available samples we measure a double peak structure observed at $2\theta = 14.7$–$15.3°$ for SC1 and $2\theta = 14.33$–$14.95°$ for SC2, which can be attributed to the superlattice effect, similar to reported results in Ref. [24]. Of course, these SLs are not perfect, and a certain size dispersion is expected, as deeply studied by F. Krieg et al.[22] In this sense, within the excitation volume limited by our confocal microscope, it can be found one or several domains (see illustration in Figure 1e) with a given average size, eventually leading to superradiance, as demonstrated below.

In type A SLs we have carried out μ-PL and μ-PL transients (μ-TRPL) by using the cryogenic confocal microscope setup shown in Figure 1f. In this setup, samples are held in the cold finger of a

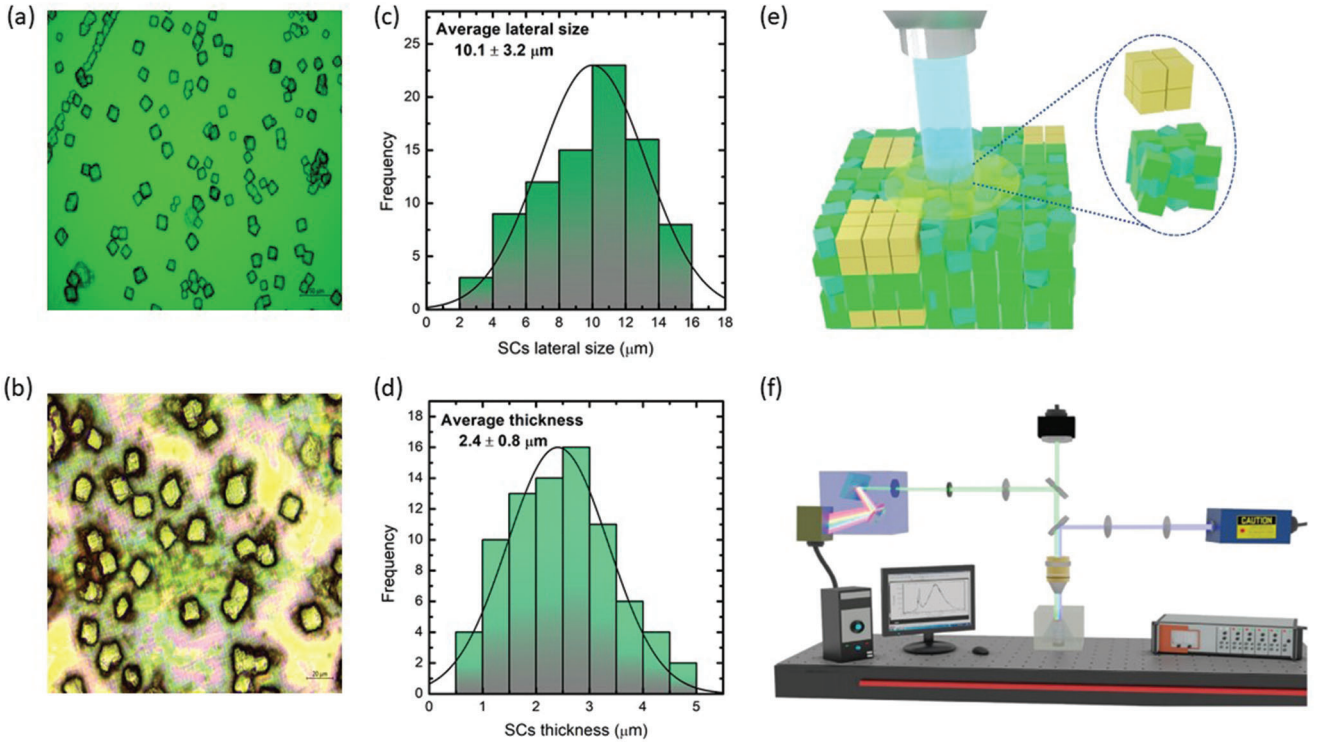

Figure 1. Optical microscope images of type A SLs used in the present work a) before and b) after metallization with gold in order to estimate the average lateral size (optical microscope) and height (profilometer), as represented in (c,d) with the corresponding histograms. e) Schematic picture regarding the light excitation/collection of a finite region of a $CsPbBr_3$ SL (bigger than the laser spot size) containing some ordered and disordered/inhomogeneous domains. f) Confocal microscopy setup for μ-PL and μ-TRPL measurements.

vibration-free closed-cycle He cryostat with the possibility to tune temperature between 4 and 300 K. A long working distance 50× microscope objective with a numerical aperture of NA = 0.42 is mounted outside the cryostat to deliver the excitation laser (a doubled fs-pulsed laser Ti:sapphire at 405 nm) to the sample and collect and send the emitted light to the spectrometer/spectrograph system (more information can be found in the Experimental Section).

In **Figure 2** we show the μ-PL spectra of four characteristic type A SLs (c-f), typically with lateral size in the range 5–10 μm, as compared to the ensemble PL spectrum of a film prepared with the same NCs (Figure 2a) and the μ-PL spectrum of background NCs in between SLs (Figure 2b). The μ-PL for single SL1 (Figure 2c) is the most repeated spectrum (similar shape) in samples made of type A SLs, and it shows a dominant low energy and narrower line at ≈2.379 eV and two higher energy contributions at 2.406 and 2.447 eV. For SL2 we have a similar situation, but an intermediate contribution cannot be deconvoluted from those at 2.38 and 2.436 eV (we will present more data below, when we describe the temperature dependent μ-PL of this SL2). In SL3 and SL4 we only observe two main and broader contributions at 2.435–2.479 eV and 2.446–2.504 eV, respectively. In contrast, the PL of the thin film (Figure 2a), which is representative of the NC size distribution, is peaked at 2.422 eV at 27 K (with a broad and weaker shoulder at higher energies), which is consistent with an average size of NCs within the fork of 6–7 nm.[46–48] More striking is the fact that background NCs exhibit a single μ-PL line peaked at ≈2.48 eV (Figure 2b), which will be consistent with smaller NC sizes in the range 5–6 nm.[47] Therefore, which is the reason to observe two or more emission contributions within the range 2.38–2.52 eV of μ-PL spectra of SLs (Figure 2c–f), as compared to the observed near single-band PL spectra measured in the film and background NCs (Figure 2a,b)?

Possibly, the self-assembling process directing the SL growth could be filtering different average NC size assemblies in a given SL. We find different possible consequences affecting the PL spectra: i) Multiple contribution from SL domains of NCs of different average sizes; ii) the effect of the background NCs emission (Figure 2b), which is centered at a peak energy (2.480 eV) appreciably higher (60 meV) than that of the average size distribution (i.e., the film in Figure 2a). One would say that the smallest NCs of the distribution will be mainly forming part of the background and some superlattices (type SL3-4 in Figure 2e,f).

Two emission contributions are typically observed in SLs prepared with $CsPbB_3$ NCs synthesized with oleic acid and oleylamine (OA/OAM) ligands, see for example Ref.[22] and others therein. In contrast, in Ref.[49] the authors obtained SLs in the order of 3–4 microns of lateral size exhibiting mainly a single emission line (eventually with a visible shoulder on its low energy side) redshifted by ≈20 meV with respect to the PL peak energy measured in a PMMA-nanocrystal nanocomposite (as a definition of the characteristic emission energy of the NC size distribution); the authors attributed such redshifted emission line to a SR state formed by dipole-dipole coupling.

As a first working hypothesis, let us attribute the lowest energy and narrower emission line (namely LEC, from "Low Energy

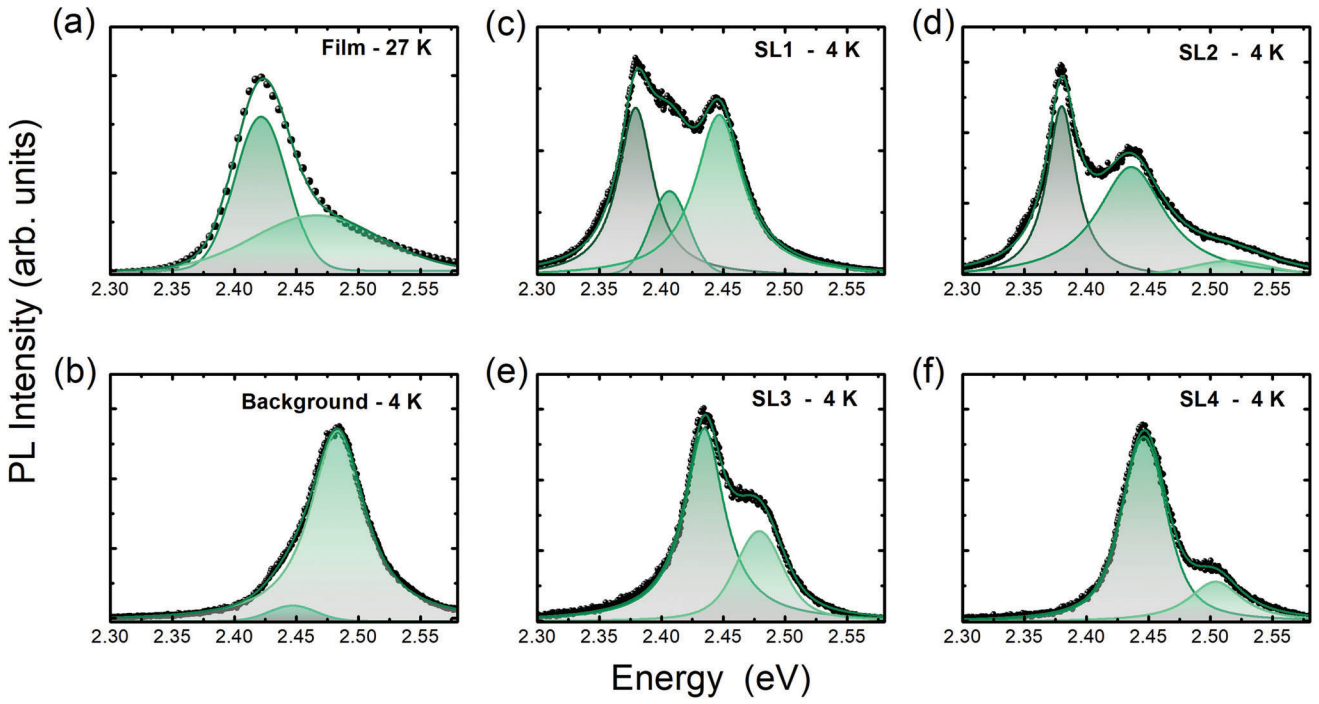

Figure 2. (a) Ensemble-PL measured (with a spectrofluorometer Edinburgh FLS1000) at 27 K in a film prepared by dipping the substrate in the same solution of $CsPbB_3$ NCs used for the fabrication of type A SLs. b–f) μ-PL spectra registered in the background of NCs (as a thin film in between SLs) (b) and several selected type A SLs: SL1 (c), SL2 (d), SL3 (e) and SL4 (f).

Contribution") observed in our type A SLs to the superradiance exciton state due to some long range coupling mechanism between NCs, to be further addressed in the Discussion section, for example due to dipole-dipole coupling, where the optical dipole corresponds to the excitonic transition, and the expected redshift due to this coupling was estimated to be ≈16 meV for NCs with edge length of 8.2 nm.[49] If such a coupling mechanism exists, one would find an increase of the redshift energy for LEC by reducing the size of the NCs, which would influence the coupling energy from two sides, the increase of the optical dipole and the increase of dipole-dipole interaction due to a reduction in the SL period (the distance between exciton dipoles). In fact, this seems to be the case, because we can estimate an energy <30 meV for the SLs with the lowest energy contribution at ≈2.38 eV and the next high energy contribution (namely HEC) at ≈2.41 eV (domain with uncoupled NCs within the same excitation volume and partially quenched due to the formation of the SR extended state), whereas the redshift would increase to 44 and 58 meV for SL3 and SL4, respectively, because the average sizes for HECs at 2.479 and 2.506 eV are clearly associated to smaller size (uncoupled) NCs. Of course, further investigations will be addressed in the future to deepen into the study of the size filtering effect in the self-assembling process of SLs with different sizes and its influence in their emission at single level.

Next experiments will be addressed in type B SLs, where bigger NCs were used, in the range 6–9.5 nm, approximately, as shown in Figure S3a, Supporting Information. These NCs were used to prepare the type B SLs, as also a dense film whose characteristic micro-PL spectrum (black curve) is shown in Figure S3b, Supporting Information, together with the frequency histograms (grey-green bars) of micro-PL peak energies measured in 100 single $CsPbBr_3$ NCs measured in a low-density film (well separated NCs). Clearly, the micro-PL peak energies measured for the single NCs spread over practically the entire PL of the dense film, 2.30–2.40 eV, with the most probable value similar to that observed for the film that takes place at ≈2.35 eV, which is consistent with an average size in the range 8–9 nm (see for example[50]). Moreover, similarly to previous samples, a relatively large inhomogeneity is present in film samples, because the Full Width at Half Maximum (FWHM) of the PL spectrum in Figure S3b, Supporting Information, is ≈54 meV, whose origin is clearly the micro-PL peak energy dispersion measured in different single NCs at 4 K, all of them related to the NC size distribution (Figure S3a, Supporting Information).

From a rough estimation of the total confinement energy for electrons and holes, E_c, in a NC with edge length L (see Figure S4, Supporting Information and details on the calculation), the observed FWHM, if due to size fluctuations, δL, can be estimated from the expression $\frac{\partial E_c}{\partial L}\delta L$; given that $\frac{\partial E_c}{\partial L} \approx 18$ meV nm^{-1} (26 meV nm^{-1}) around L = 9 nm for m* = 0.15 m_0 (0.1 m_0), hence δL would be as large as 2–3 nm, in the same order of the measured size dispersion in Figure S3a, Supporting Information. At the same time, some of the HEC bands observed in the micro-PL spectra shown in **Figure 3**a, corresponding to different type B SLs in the overall size range 5–10 μm (see the optical microscope image of these SLs in Figure 3b), exhibit similar or even larger FWHM values (see μ-PL spectra of SLs ii-v) than that for the film. Moreover, as noted above for type A SLs, we observe several HEC contributions at different peak energies within the excitation volume of other type B SLs (see μ-PL spectra of SLs i-iii-vi). Again,

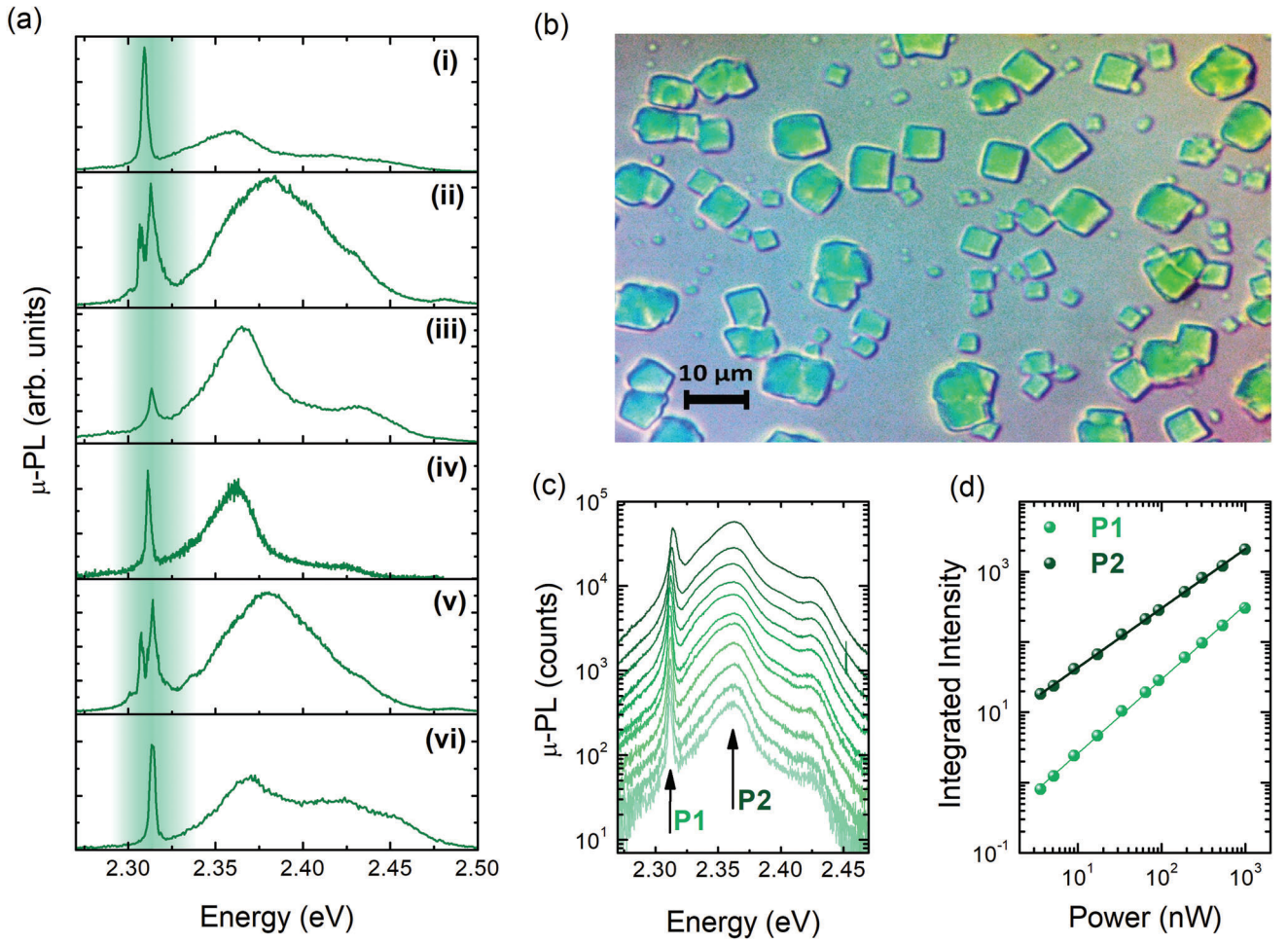

Figure 3. a) Characteristic μ-PL spectra for six different isolated SLs of $CsPbBr_3$ NCs in a type B sample at 4 K under excitation with a continuous wave laser diode at 405 nm. b) Optical microscope image of type B SLs where several of them in the range of 5-10 μm of lateral size where characterized. c) Color-coded power-dependent PL emission of $CsPbBr_3$ SLs by increasing excitation power from 25 nW (faded green) to 1 μW (black) with the same laser at 405 nm. d) Power dependence of the PL intensity integrated over the spectral emission range of the LEC and narrow peak (P1) and the dominating HEC emission band centered at around 2.365 eV (P2) for one of the type B SLs (the one in panel iv in (a)).

as we noted for type A SLs, the HEC emission in μ-PL spectra of different type B SLs are not single Gaussian bands and several contributions can be deconvoluted, hence representing several SL domains (inside the excitation volume) with slightly different average NC edge size.

More important in type B SLs is the observation of very narrow (1–5 meV) LEC peaks at energies in the range 2.305 to 2.325 eV, as can be observed in Figure S5, Supporting Information, for most measured type B SL and summarized in the histograms shown in Figure S6, Supporting Information. In some of them we observe only one LEC peak (see μ-PL spectra of SLs i-iii-iv-vi in Figure 3a) and in others two or more peaks (see μ-PL spectra of SLs ii-v in Figure 3a) and, moreover, the relative intensity of these peaks with respect to the HEC-bands varies for different SLs. The latter observation is making us more confident in our working hypothesis, in the sense that the intensity of these narrow LEC peaks could be related to the number of correlated NCs involved in the superradiance exciton state, as will be further developed in the Discussion section.

An experiment that can complete this picture is the power dependence found for the μ-PL spectra measured in the SLs, whose evolution is shown in Figure 3c for SL-iv in the range from 25 nW (faded green curve) to 1 μW (black curve). The linear fits in the log-log plot of Figure 3d for the dependencies of the integrated LEC narrow peak P_1 (≈2.315 eV) and HEC P_2 band (≈2.365 eV) reveal the slopes (exponents of the corresponding power laws) $m_{P1} = 1.07 \pm 0.01$ and $m_{P2} = 0.84 \pm 0.05$, respectively. The less than unity slope for the HEC-P_2 band would imply some dynamics related to filling shallow traps in $CsPbBr_3$ NCs (see our previous work,[51] for example). In the absence of luminescence quenching, we can use the ratio $m_{P1}/m_{P2} = 1.28$ to evidence the power recombination dynamics of the LEC peak. In fact, the slope relative magnitude that is power dependent, is further enhanced by using a pulsed laser diode (at 450 nm) that we used for the power dependent μ-PL in a SL where we observed (Figure S7a, Supporting Information) two LEC narrow lines, P_1 and P_2 (below 2.32 eV), and HEC at 2.38 eV; in this case we obtain the ratios $m_{P1}/m_{P3} = 1.35$ and $m_{P2}/m_{P3} = 1.25$ for the observed power

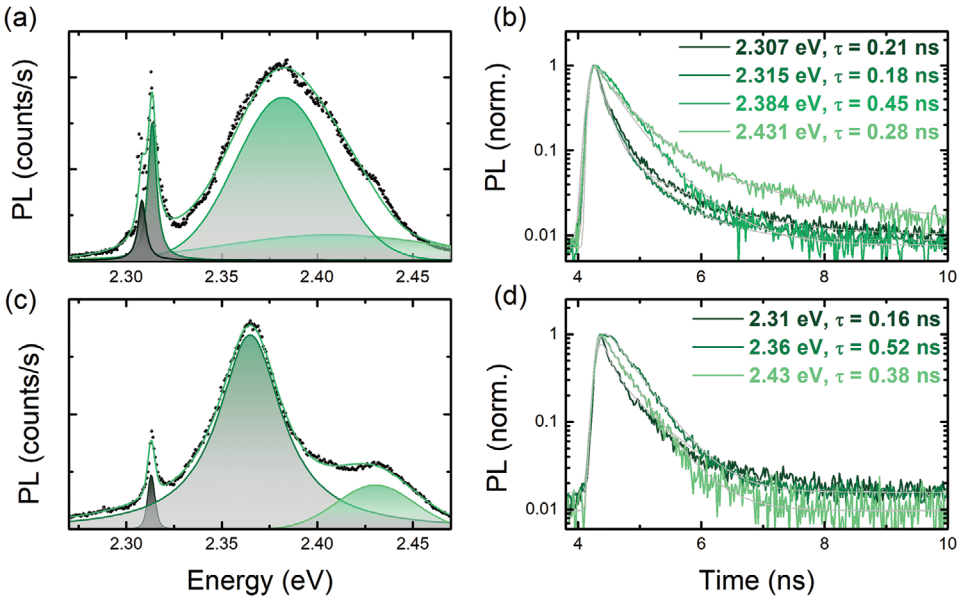

Figure 4. a–c) μ-PL spectra and b–d) transients for two characteristic type B SLs under very low power excitation (65 nW) with a ps-pulsed laser diode at 450 nm. These fits were also incorporated in the histogram of Figure S6, Supporting Information. The lifetimes in b–d were deconvoluted by using the experimental time response in Figure S10, Supporting Information (FWHM ≈ 310 ps).

dependencies in the log-log plot (Figure S7b, Supporting Information), which clearly corroborate the deviation from the linear evolution of LEC narrow lines in type B SLs and hence another element in favor of their interpretation as SR exciton states. The existence of a substructure in our LEC emission (P1 and P2 peaks) was already noted in Ref.[28] as an unresolved emission line and associated with domains of coupled NCs. Note here that in the low excitation power regime we are obtaining in most of the SLs very narrow LEC, as highlighted above (see also most of type B SL spectra in Figure S5, Supporting Information). However, the total FWHM of P_1 and P_2 peaks increases linearly with the excitation power reaching a value of 15 meV at 2 μW and saturating at 16 meV above this power (see Figure S7c and Table S1, Supporting Information). In Ref. [28], the reported linewidth for the low energy emission line was ≈15 meV under an excitation fluence >500 nJ cm^{-2}, which is equivalent to our largest μ-PL linewidth measured here under the highest excitation power condition (see Figure 2d).

The existence of different NC domains exhibiting SR emission in restricted low energy intervals inside type B SLs would be possible, because of the decreasing value of $\frac{\partial E_c}{\partial L}$ by increasing the NC edge size emitting at lower energies. Most of these LEC emitting states are located in the interval 2.305–2.325 eV (Figure S5a, Supporting Information), but we can also locate others where the LEC is observed above that interval, particularly 2.336 and 2.349 eV, as observed in Figure S8, Supporting Information. For these two SLs the energy distance to the first HEC state is 27 and 33 meV, above the values for the other type B SLs with lower energy LEC peaks, which are mostly dispersed in the range 17–27 meV. These energy distances, related to the dipole-dipole coupling energy, are consistent with the smaller values expected in type B SLs, because formed with bigger NCs in average, as compared to previous results in type A SLs (where we found energy distances of 30–60 meV), These findings will be further developed below in the Discussion section.

Interestingly, the decay times measured in SLs, both at LEC and HEC peak energies, are significantly shorter than the values measured in thin films of $CsPbBr_3$ NCs, where we measure values in the range 1.8–1.9 ns below 100 K (see Figure S9, Supporting Information), very close to values found for similar films in literature.[46,52] In type B SLs we measure lifetimes as low as 0.16–0.21 ns at LEC peak energies and 0.3–0.5 ns for HEC peak energies under very low excitation powers, as shown in **Figure 4**. In type A SLs the lifetimes measured for both LEC and HEC are also very similar, but in the range 0.4–0.5 ns, as will be described below in **Figure 5**.

Therefore, if we compare those LEC lifetimes with the exciton recombination time in the thin film (where a random distribution of NCs with different sizes is expected), the radiative rate for these exciton states is accelerated by around a factor 4 and 10 in type A and B SLs, respectively. This important reduction of the lifetime is another feature which is compatible, but not conclusive, with the identification of SR emission.[23] The longer LEC lifetime in type A SLs can be due to its more important inhomogeneous character (linewidths in the range 20–30 meV, because $\frac{\partial E_c}{\partial L}$ is greater than its value for type B SLs). The fact that the HEC lifetimes in SLs were also short (0.3–0.5 ns in both type A and B SLs and different peak energies) will deserve further explanation in the Discussion section.

Finally, we have considered a third type of SLs (C), this time made by alloyed $CsPbBrI_2$ NCs, whose emission spectra is also exhibiting inhomogeneously broadened LEC lines at ≈1.997–2.019–2.028 eV for SL-C1-2-3 with FWHMs in the range 25–35 meV and HEC bands from 2.05 to 2.13 eV, as shown in Figure S11, Supporting Information. Let us consider this type C SLs as a further illustration of a strong inhomogeneous nature

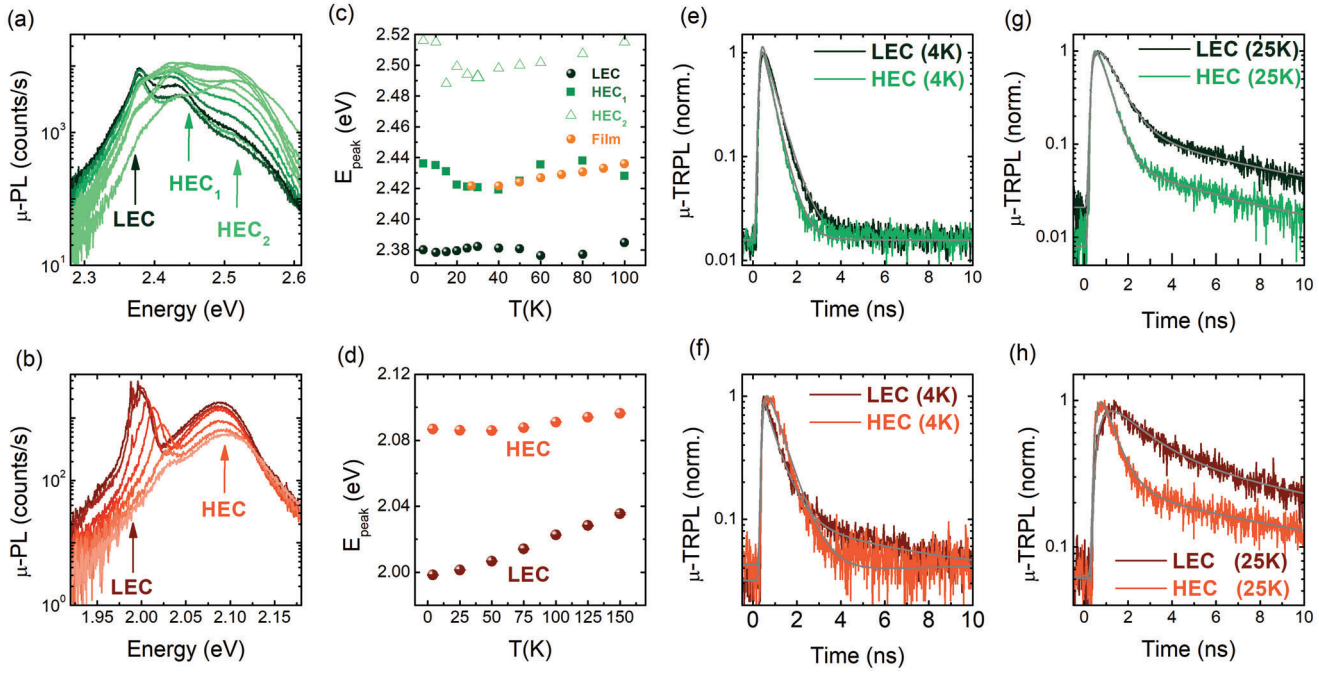

Figure 5. μ-PL spectra of a) $CsPbBr_3$ type A and b) $CsPbBrI_2$ type C SLs as a function of temperature in the ranges 4–100 and 4–150 K, respectively. Temperature dependence of the deconvoluted LEC and HEC peak energies in c) type A and d) type C SLs. μ-TRPL spectra in the same SLs at e,f) 4 K and g,h) 25 K. In type A SLs, the transients plotted as dark-green for LEC and light-green for HEC were fitted at 4 K with τ_{LEC}(4 K) = 0.54 ns and τ_{HEC} (4 K) = 0.44 ns, whereas at 25 K τ_{LEC}(25 K): τ_1 = 0.68 ns, τ_2 = 5.52 ns and τ_{HEC}(25 K): τ_1 = 0.42 ns, τ_2 = 5.08 ns, with 405 nm pulsed fs laser. Similarly, in type C SLs, the transients plotted as dark brown for LEC and orange for HEC were fitted with τ_{LEC}(4 K): τ_1 = 0.65 ns, τ_2 = 6.03 ns and τ_{HEC}(4 K): τ_1 = 0.72 ns, τ_2 = 4.02 ns, whereas at 25 K τ_{LEC}(25 K): τ_1 = 1.75 ns, τ_2 = 10.97 ns and τ_{HEC}(25 K): τ_1 = 0.62 ns, τ_2 = 8.51 ns, with 450 nm ps pulsed laser.

of the LEC emission, in the same order of that observed in type A SLs, in this case due only to fluctuations in the NC edge length, but now for type C SLs suffering additionally of compositional fluctuations (Br-I content within each NC). Both inhomogeneities makes more difficult the study of these SLs, but also interesting, because of the observation of several "enhanced" ultranarrow lines within the LEC emission region (see SL-C1 in Figures S11 and S12, Supporting Information), which would be ascribed here to single NCs. Until now, the only study considering SLs made of alloyed perovskite NCs was studying photoinduced changes in the alloy composition of NCs.[24]

The last important experiment considered in the present work to support the nature of the LEC emission as superradiance, and its origin, is temperature dependent μ-PL/μ-TRPL of $CsPbBr_3$ type A and $CsPbBrI_2$ type C SLs in the diapasons of 4–100 K and 4–150 K, respectively, as shown in Figure 5. The temperature evolution of μ-PL is shown in Figure 5a,b, from which we can extract the displacement of the peak energy of LEC and HEC emission contributions as a function of temperature (Figure 5c,d). Representative μ-TRPL spectra at 4 and 25 K are included in Figure 5e,f and Figure 5g,h, respec.

For the investigated type A SL (Figure 5c) we fitted and followed with temperature a LEC Lorentzian line at 2.38 eV (LEC: dark green solid circles) and two HEC Gaussian bands at ≈1.435 eV (HEC_1: green solid squares) and 2.51 eV (HEC_2: green hollow triangles). As we indicated above (when describing μ-PL spectra measured in different type A SLs, Figure 2), we cannot resolve any lower energy HEC emission as in other single SLs, but we observe a sigmoidal behavior for this HEC_1 band where its peak energy strongly reduces with increasing T in the region 4–30 K, surely produced by an internal recombination dynamics between HEC_1 and lower energy states. It should be stressed here such a fast variation observed in a very narrow T-diapason. Above 40 K, the deconvoluted HEC_1 peak energy is following approximately the same variation as that observed in the film (orange solid circles in Figure 5c); similarly, HEC_1 peak energy increases with T above 30 K. In type A SLs we can observe well resolved the LEC line until 25–30 K (see Figure 5a) where its peak energy varies fast (dark green solid circles in Figure 5c), whereas above 30 K it is observed as a shoulder. Contrarily, in the case of the type C SLs the LEC is observed well resolved up to near 125 K and its peak energy is blue shifting faster than HEC (it varies like in a thin film of alloyed NCs, see Figure S13, Supporting Information), possibly because of a certain internal recombination dynamics due to both compositional and edge size fluctuations; note that the ultranarrow peaks disappear above 50 K.

Considering the μ-TRPL curves at 4–25 K in Figure 5e–g,f–h for type A and C SLs it is clear that increasing the temperature slows the decays observed for both LEC and HEC (see the fitting values listed in the figure caption), being this slowing more severe in the μ-PL transients of LEC (SR) states than in the case of HEC emission. In the case of the alloyed ($CsPbBrI_2$) type C SLs, the transients of HEC slow down more dramatically by increasing the temperature to 25 K, even if LEC emission is visible even above 100 K.

3. Discussion

In this section we focus on the evaluation and analysis of four main SR effects: 1) the nature of LEC emission as a SR phenomenon and its origin, 2) the SR energy shift, 3) the SR enhancement factor and correlation length as a function of the number of coupled NCs, N, and 4) the decoherence of the SR exciton state by increasing temperature, possibly due to the coupling of the SR exciton state to phonons.

In previous section, we gave several results supporting the SR nature of the LEC emission in SLs measured at T = 4 K: i) narrow LEC line at the lowest side of the SL emission, especially in type B SLs, where the NC size distribution involves nanocubes larger than 9 nm, hence with a very weak confinement leading to small confinement energy dispersion, ii) an increase of the energy difference between the LEC and the first HEC emission peak, which is correlated with the increase in the LEC (or HEC) peak energy (i.e., related to SL domains with smaller NCs and, at the same time, with reducing NC-NC distance), and iii) a strong reduction of the measured lifetime at LEC peak energies over that measured in NCs of a thin film (moreover, the LEC lifetime can be even smaller than those measured in HEC at higher energies, mostly in the case of more homogeneous type B SLs). Furthermore, we observe a clear and fast decoherence of the SR emission by increasing temperature (within the radiative range of the NC emission), as further developed below. These featuring properties, together with complementary results reported in literature, where superradiance was claimed in Ref.[49] and superfluorescence was demonstrated at that low energy states under higher pulsed excitation powers,[28] make us confident in the SR nature (delocalized exciton state throughout several NCs of the total ensemble) for the LEC emission in perovskite SLs.

Next point is the origin of such SR emission and its compatibility with the observed energy redshift for the SR line. We contemplate two possibilities: electronic and dipole-dipole coupling, as the more reliable ones. The electronic coupling inside our perovskite SLs based on NCs capped with OAM/OA ligands, even if not completely disregarded, would lead to very low redshifts/minibands, <3 meV if the average distance between NCs with 7 nm of edge size was ≈1 nm, as estimated in Supp. Info (see our comment regarding the calculation of confinement energies for Figure S4, Supporting Information). This value can be taken as an upper limit, given that OAM/OA ligands can introduce inter-NC distances larger than 2 nm and miniband width or the shift in transition energies will decrease exponentially with the barrier thickness.

The dipole-dipole coupling is a long-range interaction that was used to explain the formation of J-aggregates in molecules, which would lead to an important redshift with respect to the optical transition energy in isolated molecules.[3,7–13] In our case the J-aggregate would correspond to domains formed by a certain number of coupled NCs inside the SL. The coupling energy was recently estimated to be ≈16 meV by considering the (strong) optical dipole in NCs with 8.2 nm of edge size and 12 nm for the distance between NCs, center-to-center.[49] Therefore, long range dipole-dipole interaction is a serious candidate for the origin of the SR exciton states in perovskite SLs. Furthermore, the dipole-dipole interaction can also help to understand other observed features in the emission spectra of our SLs, because it is at the core of exciton energy transfer between NCs. This process consists in the nonradiative quenching of an exciton located in a certain NC to transfer its energy to a neighbor NC, provided their distance is sufficiently short, with a Forster-like transfer rate; such exciton transport would lead to a redshift to low energies of the whole inhomogeneous PL band representative of the NC ensemble (see the theoretical work by Lee et al.[53]).

In our SLs we have observed two main emission features, namely LEC and HEC ones, sometimes well resolved. However, in other cases we observe several HEC resolved lines/shoulders. This makes possible the existence of several domains exhibiting SR emission at different energies, but clearly only the lowest energy one will be dominating and eventually separated over a background (i.e., an inhomogeneous distribution) of uncoupled NCs (whose size/energy dispersion and distance does not allow such coupling). If we represent in a single plot the energy difference between the first HEC emission band and the LEC peak energy, δE, as a function of E_{LEC}, in most of the measured type A and B SLs we find a certain correlation, as shown in **Figure 6**a. This correlation, given that E_{LEC} contains the carrier confinement energy, means that dipole-dipole interaction between NCs increases by reducing their size (producing an increase of their optical dipole moment) and distance between them (producing an increase of their dipolar interaction). Particularly, we find δE, the dipolar coupling energy, to be ≈22 ± 5 meV (Figure 6a) for type B SLs, where the most probable $E_{\mathrm{LEC}} \approx 2.315$ eV (Figure 6a and Figure S6a, Supporting Information), and increases to the range of 40–60 meV in most of type A SLs. The dispersion is very high, possibly due to the strong dependence of $\delta E \approx R^{-3}$ (R the distance between NCs), but these results are encouraging to undertake future studies in different kinds of perovskite SLs.

At this point we can try to compare some of our experimental results with the theoretical model proposed recently by F. Mattioti et al.[54] by using the function described in this paper to fit our data:

$$\frac{\Gamma}{\gamma} - 1 = \frac{AN^B}{N^B + N_{\mathrm{sat}}^B} \tag{1}$$

where the left side of the equation is the SR enhancement factor defined by the radiative rates for SR and NCs, Γ and γ, respectively. In the right side of the equation, A, B, and N_{sat} are fitting parameters, corresponding to the saturation of the enhancement factor, the exponent for N (number of NCs in the SR state), and its saturating value, respectively. Following this work, it is interesting to note here that the enhancement factor of the SR state is not increasing proportionally to N, because it is necessary to take into account the thermal decoherence introduced by lattice vibrations at a finite temperature and the inhomogeneous broadening of the SR transition originated by the structural disorder in the SL.

The most appropriate procedure to extract the enhancement factor in Equation (1) would be based on transient μ-PL measurements at the different peak energies of interest. However, it would be necessary to have an experimental system with sufficiently short temporal response. In our case, as described above, we can deconvolute lifetimes larger than 50 ps and hence the measured values for SR lines, in the range 160–210 ps for type B SLs (Figure 4b–d), has an appreciable error. In any case, if we compare these rates (4.8–6.3 ns^{-1}) with the inverse of the lifetime

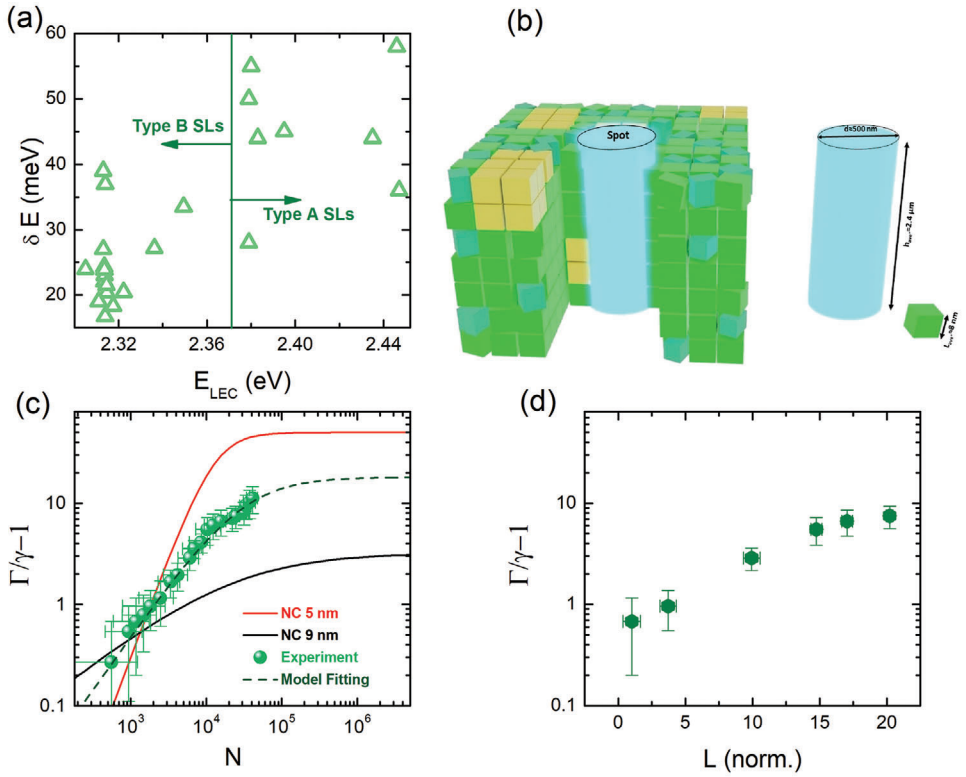

Figure 6. a) Energy difference between the first HEC emission band and the LEC peak energy, δE, as a function of E_{LEC} for type A and B SLs. b) Schematic picture representing the light excitation/collection spot within a $CsPbBr_3$ SL. SR enhancement factor as a c) function of N and d) the normalized correlation length in the SL (with disorder) under low excitation power (≈50 nW) at 4 K.

measured in films of uncoupled ensembles of our NCs (1/1.9 = 0.53 ns^{-1}), we would estimate an enhancement factor $\frac{\Gamma}{\gamma} - 1$ in the range of 8–11. Here we also propose to estimate the experimental enhancement by a very simple and faster method: the ratio between the integrated intensity of the SR line and that of the HEC emission in the same energy range, both quantities extracted from the fittings made for the μ-PL spectra registered under low excitation power (see Figure S14, Supporting Information) for twenty different SLs at 4 K. This method can be sufficiently precise if the SR line is mostly homogeneous, as occur for type B SLs under very low excitation powers (see the effect of power on the enhancement factor in Figure S14a, Supporting Information). It is worth to note that we obtain with this method an enhancement factor similar to that obtained from the ratio of experimental lifetimes in two of the SLs.

Next step is the evaluation of the number of NCs within the laser excitation volume inside the SL (see illustration in Figure 6b) by considering several approximations. If the LEC emission is due to the SR state, then the SR/HEC photon emission rate would scale as $N^2/N = N$,[14,37] where N is the number of single emitters (NCs). For type B SLs, the SR emission was very localized in energy (1–5 meV) at around the most probable value 2.315 eV, and in space, being a domain with size much smaller than the wavelength of light. Therefore, we can roughly estimate the number of NCs producing the SR emission in the SL as the ratio between the integrated intensity of the narrow SR line (I_{SR}) and the expected total emitted PL power (P_{PL}) if all the light in the spot was produced by HEC emission. Here we consider that our excitation spot overlaps with our collection spot. Next, we include all the experimental efficiency factors that need to be taken into account to use the final measured SR Intensity (I_{SR-M}) in the CCD: the finite numerical aperture (η_{NA}), efficiency of the fiber coupling (η_{Fiber}), efficiency of the monochromator grating (η_{Grat}), efficiency of the CCD (η_{CCD}). Finally, we also take into account the sample absorption and the measured quantum yield (1 at low T) of the sample. Following these approximations, the estimation of the number of NCs active in our spot size giving rise to the SR emission can be expressed as:

$$N = \left(N_{SR}\right)_{spot} \cong \frac{I_{SR}}{P_{PL}} \cong \frac{I_{SR-M}}{\eta_{\alpha}\eta_{QY}\eta_{NA}\eta_{Fiber}\eta_{Grat.}^{2}\eta_{CCD}P_{exc.}} \quad (2)$$

where we considered the absorbed power in the SL from the incident excitation power

$$P_{abs.} = P_{exc.}\ (1 - e^{-\mu z}) = P_{exc.}\ \eta_{\alpha} \quad (3)$$

where μ is the intrinsic absorption coefficient for $CsPbBr_3$ NCs which we got from the Ref. [55] considering the excitation wavelength. In equation 2 we combined $P_{exc.}\eta_{\alpha}$ with the remaining parameters. In any case, our estimation of N should be considered as a rough evaluation, as we do not have any direct

measurement of the number of coupled NCs inside the excitation volume participating in the SR emission.

Now we can represent the experimental $\frac{\Gamma}{\gamma} - 1$ as a function of the estimated N with equation (2) for the 20 measured SLs (green solid circles in Figure 6c). Red and black continuous lines in Figure 6b, stand for the curves obtained from Equation (1) representing the model prediction in Ref. [54] for NCs with edge sizes of 5 and 9 nm, respectively. The best fit to our experimental data (green dashed line in Figure 6c) results in A = 18, B = 1.07 and N^{B}_{sat} = 40000. This fit is consistent with a NC size in the range between 5 and 9 nm, which are compatible with our measured NC size distribution (see Figure S3a, Supporting Information).

The total number of NCs contributing to the PL emission in the collection spot of our confocal setup (Figure 6b), the spot size defined using the lateral resolution of the confocal configuration ($d_{\text{lat.}} = 0.4\frac{\lambda}{NA}$). Considering our PL emission $\lambda = 530$ nm and numerical aperture (NA) = 0.42, our spot size will be d ≈ 505 nm (r = (d/2) ≈ 250 nm), and if we consider the average nanocube size ≈8 nm, we can estimate roughly the total number of nanocrystals by dividing the spot volume to the volume of a single nanocube ($N_{\text{total}} = \frac{Spot_{\text{volume}}}{NC_{\text{volume}}}$). In this estimation to calculate the spot volume the height (h_{SL}) of the SLs was considered in the range 1.25–2.4 μm, that is, whose lateral size ranged 5–10 μm (see Figure 1d). The value of N_{total} is ≈12–23 times higher than the saturation value of NCs ($\frac{N_{\text{total}}}{N_{\text{sat}}} \approx 12 - 23$) contributing to the SR emission. Therefore, most of the NCs in the excitation volume are uncoupled and forming part of the HEC emission.

Since we suggest that the mechanism responsible for the formation of SR emission in our SLs is the same as in the case of the molecular J-aggregates, we can evaluate the delocalization (correlation) length L of a SR state based on J. Knoester's model[10] by the comparison of the linewidths extracted from LEC and HEC emission lines. Figure 6d shows the SR emission enhancement factor as a function of the normalized correlation length (L) in relative units for six different SLs (with different enhancement factors). According to this figure, it is obvious that the enhancement factor increases when the correlation length increases, and a relative increase of about 20 times in the correlation length is associated with an increase of nearly one order of magnitude in the enhancement factor.

The mathematical explanation for the narrowing of the linear absorption spectrum of J-aggregates and its relation to the correlation length can be given by taking into account the probability distribution of each exciton energy to first order in the molecular disorder.[56] Each aggregate consists of a linear chain of N equidistant nonpolar two-level absorbers with parallel transition dipoles of magnitude μ. The electronic states of an aggregate are described by the Frenkel exciton Hamiltonian.[57]

$$\hat{H}_0 = \hbar \sum_{n=1}^{N} \left(\omega_0 + d_n\right) \hat{B}_n^{\dagger} \hat{B}_{n+1} + \hbar \sum_{n=1}^{N-1} V \left(\hat{B}_n^{\dagger} \hat{B}_{n+1} + \hat{B}_{n+1}^{\dagger} \hat{B}_n\right) \quad (4)$$

Here $\hat{B}_n$ and $\hat{B}_n^{\dagger}$ denotes the Pauli annihilation and creation operators for an excitation on molecule n, respectively, and $(\omega_0 + d_n)$ is the transition frequency of molecule n, where ω_0 is the average transition frequency and d_n is a static random offset which describes diagonal disorder. Finally, V is the nearest-neighbor interaction, which is negative for J-aggregates. V is assumed to be homogeneous; interactions between different aggregates that could be present in the excitation volume are neglected. Considering the following Gaussian joint distribution for the molecular frequency offsets of a single aggregate:

$$\bar{P}^{(N)}\left(d_1, \ldots, d_N\right) = \frac{1}{(2\pi)^{N/2}\sqrt{\det\left(A\right)}} \times \exp\left(-\frac{1}{2}\sum_{n,m=1}^{N} A_{nm}^{-1} d_n d_m\right) \quad (5)$$

where A_{nm}^{-1} denotes the nm element of the inverse of the covariance matrix $A_{nm} \equiv \langle d_n d_m \rangle = a_0^2 \exp(-|n-m|/L)$, also, a_0 and L give the amplitude and correlation length of the molecular disorder (L in units of the lattice constant), where more mathematical details can be found in ref. [10]. Note that a_0 equals the standard deviation of the Gaussian marginal distribution for the frequency offset of a single molecule. This procedure predicts a narrowing of the local (molecular) disorder if the molecular transition frequencies on each aggregate are entirely uncorrelated to each other:

$$\sigma \approx \sqrt{\frac{1-\beta}{1+\beta}} a_0 \left[\frac{3}{2\left(N+1\right)}\right]^{1/2} \quad (6)$$

where $\beta \equiv \exp(-1/L)$ indicates the degree of correlation between the transition frequencies of molecules within a single chain (J-aggregate), and a_0 is the standard deviation of a Gaussian distribution. This expression is valid for $\beta^N \ll 1$, where N is the number of molecules per aggregate. Therefore, by increasing the number of molecules in the aggregate the narrowing should be more important. In equation (6) σ and a_0 can be extracted directly from the linewidths of LEC (SR) peaks (especially narrow in the case of type B SLs) and HEC (uncoupled NCs) broad bands inside the excitation volume of the μ-PL spectra, respectively. Moreover, we use in equation (6) the N value deduced above from Equation (2). The consequence of equation (6) is the relationship between the SR and HEC linewidths and the correlation length, which is demonstrated in our SLs following our estimation of N (Figure 6d).

Next, we analyze in more detail the temperature evolution of SR and HEC spectra (Figure 5). By increasing the temperature, in addition to the bandgap variation (Figure 5c,d), the coherent dipole-dipole coupling of NCs should be lost, as predicted in Ref. [54]. The increase in temperature causes an important reduction of the SR emission intensity in both type A ($CsPbBr_3$) and C ($CsPbBrI_2$) SLs, as observed in the Arrhenius plots of **Figure 7**a,b (black and brown solid circles). This intensity reduction is in close correspondence with the slowdown of the PL transients (increase of lifetimes), as discussed below, and it should contain the origin of the thermal decoherence mechanism. For type B $CsPbBr_3$ SLs, the μ-PL measurements were performed several weeks later and an important aging effect was observed, even if the samples were conserved in vacuum (and darkness). Now the LEC peak energy is shifted to 2.30 eV and the line is particularly broad as compared to fresh SLs (see Figure S15, Supporting Information), hence we cannot exclude the presence of bulk microcrystals (by coalescence of NCs with time) in these aged type B SLs, as recently reported in.[23] In spite of this aging effect, the temperature

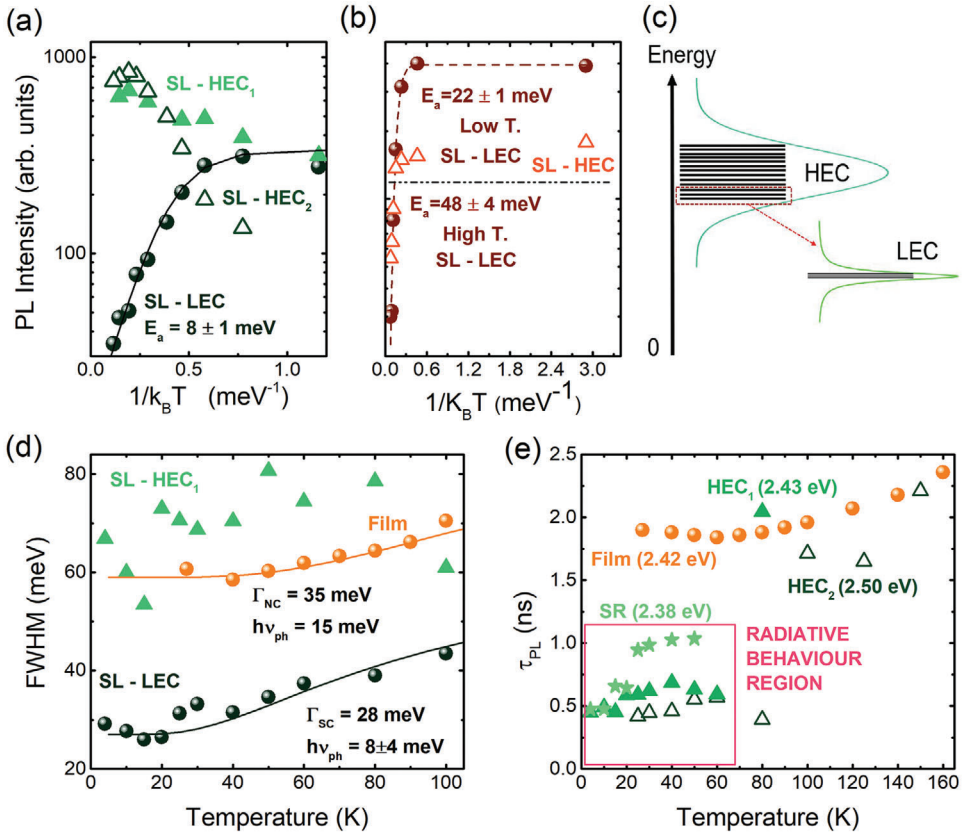

Figure 7. Arrhenius plots of the integrated emission intensity of LEC and HEC for a) $CsPbBr_3$ and b) $CsPbBrI_2$ SLs; the LEC intensity variation was fitted with activation energies of 8 and 22 meV (48 in the whole temperature range) for $CsPbBr_3$ and $CsPbBrI_2$ SLs, respectively. c) Schematic picture illustrating the HEC states related to an inhomogeneous ensemble of NCs and the SR state formed from a small domain of this ensemble. Temperature evolution of LEC and HEC d) linewidths and e) lifetimes; orange solid circles stand for the FWHM of emission spectrum and lifetime measured in a thin film made with the same NCs used for obtaining type A SLs.

behavior (Figure S16, Supporting Information) is not far from that observed in fresh SLs shown in Figures 5 and 7a,b.

In the case of the type A $CsPbBr_3$ SL the experimental Arrhenius plot in Figure 7a can be fitted with an activation energy $E_a = 8 \pm 1$ meV. This activation energy should be ascribed to the thermal decoherence of the dipole-dipole interaction, whose origin can be due to exciton-phonon interaction, as suggested in Ref. [49]. A direct ionization of the SR exciton state into the NC ensemble (see illustration in Figure 7c) would not be reliable, because E_a is smaller than δE (>30 meV for type A SLs, after Figure 6a). It is worth to note here that the estimation of the dipole-dipole interaction in Ref. [54] yielded much smaller values. In our experimental estimations for δE and that estimated in Ref.[49] (≈20 meV, as obtained from the peak energy of the PL measured in the SL and that of a polymer-NC nanocomposite), the exciton-phonon interaction is the most reliable decoherence mechanism with temperature. In fact, the SR line exhibits a strong broadening with temperature above 20 K (black solid circles in Figure 7d) that can be easily fitted with the phonon occupation function (see our previous work on single NCs[19]):

$$\Gamma_{SR} \cong \Gamma_{SR}^{0} + \frac{\gamma_{ph}^{SR}}{e^{\frac{\hbar\omega_{ph}}{kT}} - 1} \quad (7)$$

The fitting (black continuous line in Figure 7d) was done with an effective phonon energy $\hbar\omega_{ph} \approx 8$ meV (with high estimation error, ≈4 meV) and an exciton-phonon coupling constant of $\gamma_{ph}^{SR} \approx 28$ meV. In the film (introduced in Figure 7d as orange solid circles for comparison purposes) the best fit gives a higher phonon value, close to the LO one (16 meV), and similar exciton-phonon coupling constant, as also in Ref. [49]. A lower effective phonon energy is possible due to the folding effect in the acoustic phonon dispersion curve due to the SL periodicity. This phonon energy is compatible with the activation energy obtained for the SR intensity reduction (8 meV), hence the strong coupling of the SR-exciton state with phonons should be the most reliable mechanism of the strong SR thermal decoherence in the range 4–70 K, approximately.

Above 25 K, the thermal decoherence of the SR exciton state (intensity decreases, linewidth and lifetime increase) is being transformed into excitons localized in the ensemble of uncoupled NCs (inside the excitation volume) and hence feeding the HEC states, provided that radiative recombination dominates in the SL system. In fact, an increase of intensity is observed for both HEC emission bands up to 60–70 K, well correlated with the observed intensity decrease of SR. Above 60–70 K, HEC emission also begins to decrease, which is ascribed to the participation of

trapping-detrapping mechanism in $CsPbBr_3$ NCs (see our previous work in this field[51]) and the activation of some nonradiative recombination channel: see the decrease of intensity observed in thin films above 100 K (Figure S9b, Supporting Information). This is also the case in the type C $CsPbBrI_2$ SL, where the intensity for both LEC and HEC emission lines decrease. The activation of nonradiative recombination channels above 25 K possibly influences the thermal decoherence of the SR exciton state above that temperature (its main lifetime passes from 0.65 ns at 4 K to 1.75 ns at 25 K, see Figure 5f–h). This is possibly the reason why we deduce a slope as large as 22 meV until 75 K (48 meV if we consider the total temperature range, 4–150 K) for the temperature variation of the LEC line (Figure 7b). The added effect of composition and edge size fluctuations in the ensemble of NCs can contribute to the faster thermal decoherence observed in these SLs as compared to those made of $CsPbBr_3$ NCs.

Finally, let us to add some more interesting features related to the temperature evolution of the emission in $CsPbBr_3$ SLs, at least in the temperature range 4–70 K where the excitonic recombination in the SL is predominantly radiative (region squared in Figure 7e):

i) (4–20 K) the SR exciton state of this SL maintains a strong coherence, which is characterized with short lifetimes ≈0.45–0.7 ns.
ii) (25–50 K) the linewidth of the SR line increases and its intensity decreases due to the exciton-phonon interaction responsible of the SR thermal decoherence. The lifetime increases up to 0.9–1.1 ns.
iii) from 4 to 60 K the fast decay measured in HEC states varies slightly in the range 0.45 to 0.65, approximately, and above 80 K abruptly increases until values very similar to those measured in the film (orange solid circles in Figure 7e).

The last result is particularly interesting, because it means that Förster exciton-energy transport is still taking place until the SR is totally quenched at 80–90 K. Above this temperature, the exciton recombination dynamics in the SL does not differ from that of a thin film. It should be notice that D. D. Blach et al. did a similar observation for the lifetime measured in the whole SL emission band of their perovskite SLs above 75 K.[49]

4. Conclusion

To summarize, the investigation of the self-assembly of cubic-shaped $CsPbBr_3$ and $CsPbBrI_2$ NCs into cuboidal superlattices was carried out and superradiance emission of NCs in certain SL domains was studied in three types of SLs by means of confocal PL microscopy. In the case of $CsPbBr_3$ SLs we have measured very narrow (1–5 meV) emission lines on the low energy side of their μ-PL spectra (LEC lines), which can be considered near homogeneous, and characterized by lifetimes as short as 160 ps. The enhancement factor estimated from the integrated intensity of these LEC lines (divided by the emission background of uncoupled NCs in the same emission region) can reach values as high as 10, similar to the value estimated from the ratio of lifetimes measured in a film and that of the LEC, which are associated to domains of nearly identical NCs (at least in their emission energy) formed by 1000 to 40 000 NCs within the micrometric SLs, as estimated in our work. Therefore, the nature of the LEC line is consistent with a SR exciton state whose origin is due to the coupling of optical dipoles in perovskite NCs, as in molecular J-aggregates; this origin is consistent with our estimate of the correlation length for these SL domains with correlated NCs. The coherence of the SR exciton state has been studied in the temperature region dominated by a radiative recombination dynamics (from 4 to 70–80 K, in the studied SL). The importance of thermal decoherence for the SR state is observed above 25 K and due to its coupling with an effective phonon energy of ≈8 meV. The emission of high energy states in the SL spectra are also characterized by short lifetimes, because of Förster transfer of energy (from small to large NCs of the distribution or from high to low emission energies) in the SL. These findings are encouraging to undertake future studies in SLs based on NCs with different average edge size, perovskite composition, SL period and total size. Particularly, μ-PL studies in a statistically representative number of SLs will be needed to extract the correct information about the formation of the SR exciton state in the different SL systems and evaluate their limitations for using them in different applications (photonics, exciton transport, quantum technologies, etc.).

5. Experimental Section

Synthesis of Colloidal Solution: $CsPbBr_3$ NCs were synthesized using the hot-injection approach reported by Kovalenko and colleagues,[58] with some modifications[56] All of the reactants were utilized just as they were received, with no extra purification. In brief, Cs-oleate solution was prepared by mixing 0.41 g of Cs_2CO_3 (Sigma-Aldrich, 99.9%), 1.25 mL of oleic acid (OA, Sigma-Aldrich, 90%), and 20 mL of 1-octadecene (1-ODE, Sigma-Aldrich, 90%) were loaded together into a 50 mL three-neck flask at 120 °C under vacuum for 1 h under constant stirring. Then, the mixture was N_2-purged and heated at 150 °C to reach the complete dissolution of Cs_2CO_3. The solution was stored under N_2, keeping the temperature at 100 °C to prevent Cs-oleate oxidation. For the synthesis of $CsPbBr_3$ and $CsPbBrI_2$ PNCs, 1.0 g of $PbBr_2$ (ABCR, 99.999%), and the corresponding $PbBr_2/PbI_2$ mixture, were mixed with 50 mL of 1-ODE into a 100 mL three-neck flask. The mixture was degassed and heated at the same time at 120 °C for 1 h under constant stirring. Then, a mixture of 5 mL each of both pretreated (130 °C) OA and oleylamine (OLA, Sigma-Aldrich, 98%) were separately added to the flask under N_2, and the mixture was quickly heated at 170 °C. Simultaneously, 4 mL of Cs-oleate solution was injected into the mixture quickly and then, the reaction was quenched to immerse the mixture into an ice bath for 5 s. In order to perform the isolation process of PNCs, the colloidal solutions were centrifugated at 4700 rpm for 10 min. Then, PNCs pellets were separated after discarding the supernatant and redispersed in toluene to concentrate the PNCs at 100 mg mL^{-1}.

Growing 3D Superlattices: $CsPbBr_3$ and $CsPbBrI_2$ NC SLs were grown on glass substrates, which was preliminary cleaned by following the procedure reported in ref.[57] before the self-assembly process. In a standard assembly procedure, the substrate was put into a Teflon well and 10 μl of colloidal solution in toluene were dropped onto the substrate. The well was subsequently capped with a glass plate, and the toluene was permitted to gently evaporate. After the full evaporation of the toluene, 3D SLs of $CsPbBr_3$ and $CsPbBrI_2$ NCs were grown. Individual SLs typically had lateral dimensions between 1 and 10 μm, with some of them arranged into clusters of several SLs and others staying separated from one another in distance to make it possible for PL measurements to be done on a single superlattice.

Optical Spectroscopy and Confocal Optical Microscopy: All low temperature measurements were taken using a standard micro-PL setup, with the samples held in the cold-finger of a vibration-free closed-cycle cryostat (AttoDRY800 from Attocube AG). The sample was excited using a continuous wave (pulsed) excitation laser at a wavelength of $\lambda = 405$ nm

(450 nm), returning spectral (time resolved) PL measurements. Moreover, the alignment of the collection and excitation spots was done separately for $CsPbBr_3$ and $CsPbBrI_2$ NCs by single-mode fiber-coupled continuous wave lasers at wavelengths of $\lambda = 532$ and 660 nm, respectively. In both excitation and detection, single mode optical fibers will serve as confocal pinholes. Excitation and detection were carried out using a 50× long-working distance microscope objective with a numerical aperture of NA = 0.42 that was positioned outside the cryostat. The emission from the sample was long-pass filtered, dispersed by a double 0.3 m focal length grating spectrograph (Acton SP-300i from Princeton Instruments) and detected with a cooled Si CCD camera (Newton EMCCD from ANDOR) for recording PL spectral and with a SPAD detector (from Micro Photon Devices) connected to a time correlated single photon counting electronic board (TCC900 from Edinburgh Instruments) for time resolved PL measurements.

Supporting Information

Supporting Information is available from the Wiley Online Library or from the author.

Acknowledgements

Financial support from the Spanish Ministry of Science (MICINN) through project no. PID2020- 120484RB-I00 is gratefully acknowledged. G.M.M. also thanks the support from the Spanish MICINN & AEI (project RTI2018-099015-J-I00). I.M.S. thanks the funding of MCIN/AEI/10.13039/501100011033 with the project STABLE PID2019-107314RB-I00. S.G. acknowledges her "Grisolia" grant from Generalitat Valenciana, and G.M.M. thanks the Ramon y Cajal programme (contract RYC2020-030099-I). Thanks are also due to Dr. Raúl Iván Sánchez Alarcón for his help with X-ray diffraction characterization of NC films and SLs.

Conflict of Interest

The authors declare no conflict of interest.

Data Availability Statement

The data that support the findings of this study are available from the corresponding author upon reasonable request.

Keywords

confocal optical microscopy, lead halide perovskites, microphotoluminescence, superradiance, thermal decoherence

Received: October 21, 2022
Revised: April 3, 2023
Published online: May 19, 2023

[1] R. H. Dicke, *Phys. Rev.* **1954**, *93*, 99.
[2] R. Bonifacio, L. Lugiato, *Phys. Rev. A* **1975**, *11*, 1507.
[3] F. C. Spano, *Acc. Chem. Res.* **2010**, *43*, 429.
[4] C. Bradac, M. T. Johnsson, M. van Breugel, B. Q. Baragiola, R. Martin, M. L. Juan, G. K. Brennen, T. Volz, *Nat. Commun.* **2017**, *8*, 1205.
[5] M. Scheibner, T. Schmidt, L. Worschech, A. Forchel, G. Bacher, T. Passow, D. Hommel, *Nat. Phys.* **2007**, *3*, 106.
[6] J. Q. Grim, A. S. Bracker, M. Zalalutdinov, S. G. Carter, A. C. Kozen, M. Kim, C. S. Kim, J. T. Mlack, M. Yakes, B. Lee, D. Gammon, *Nat. Mater.* **2019**, *18*, 963.
[7] S. De Boer, D. A. Wiersma, *Chem. Phys. Lett.* **1990**, *165*, 45.
[8] H. Fidder, J. Knoester, D. A. Wiersma, *Chem. Phys. Lett.* **1990**, *171*, 529.
[9] T. Kobayashi, *J-Aggregates*, vol. 2, World Scientific, **2012**, https://doi.org/10.1142/8226.
[10] J. Knoester, *J. Chem. Phys.* **1993**, *99*, 8466.
[11] V. Malyshev, *J. Lumin.* **1993**, *55*, 225.
[12] L. D. Bakalis, J. Knoester, *J. Lumin.* **2000**, *87*, 66.
[13] G. Y. Guralchuk, I. K. Katrunov, R. S. Grynyov, A. V. Sorokin, S. L. Yefimova, I. A. Borovoy, Y. V. Malyukin, *J. Phys. Chem. C* **2008**, *112*, 14762.
[14] M. Gross, S. Haroche, *Phys. Rep.* **1982**, *93*, 301.
[15] P. K. Nayak, S. Mahesh, H. J. Snaith, D. Cahen, *Nat. Rev. Mater.* **2019**, *4*, 269.
[16] F. Yan, S. T. Tan, X. Li, H. V. Demir, *Small* **2019**, *15*, 1902079.
[17] J. Yao, L. Xu, S. Wang, Z. Yang, J. Song, *Nanoscale* **2022**, *14*, 13990.
[18] G. Raino, G. Nedelcu, L. Protesescu, M. I. Bodnarchuk, M. V. Kovalenko, R. F. Mahrt, T. Stoferle, *ACS Nano* **2016**, *10*, 2485.
[19] H. P. Adl, S. Gorji, G. Muñoz-Matutano, I. S. Alarcón, R. Abargues, A. F. Gualdron-Reyes, I. Mora-Seró, J. P. Martínez-Pastor, *J. Lumin.* **2021**, *240*, 118453.
[20] G. Rainó, N. Yazdani, S. C. Boehme, M. Kober-Czerny, C. Zhu, F. Krieg, M. D. Rossell, R. Erni, V. Wood, I. Infante, M. Y. Kovalenko, *Nat. Commun.* **2022**, *13*, 2587.
[21] I. Cherniukh, G. Rainó, T. Stöferle, M. Burian, A. Travesset, D. Naumenko, H. Amenitsch, R. Erni, R. F. Mahrt, M. I. Bodnarchuk, M. V. Kovalenko, *Nature* **2021**, *593*, 535.
[22] F. Krieg, P. C. Sercel, M. Burian, H. Andrusiv, M. I. Bodnarchuk, T. Stoferle, R. F. Mahrt, D. Naumenko, H. Amenitsch, G. Raino, M. V. Kovalenko, *ACS Cent. Sci.* **2021**, *7*, 135.
[23] D. Baranov, A. Fieramosca, R. X. Yang, L. Polimeno, G. Lerario, S. Toso, C. Giansante, M. D. Giorgi, L. Z. Tan, D. Sanvitto, L. Manna, *ACS Nano* **2020**, *15*, 650.
[24] M. C. Brennan, S. Toso, I. M. Pavlovetc, M. Zhukovskyi, S. Marras, M. Kuno, L. Manna, D. Baranov, *ACS Energy Lett.* **2020**, *5*, 1465.
[25] H. Huang, M. W. Feil, S. Fuchs, T. Debnath, A. F. Richter, Y. Tong, L. Wu, Y. Wang, M. Doblinger, B. Nickel, *Chem. Mater.* **2020**, *32*, 8877.
[26] C. Zhou, Y. Zhong, H. Dong, W. Zheng, J. Tan, Q. Jie, A. Pan, L. Zhang, W. Xie, *Nat. Commun.* **2020**, *11*, 1.
[27] S. Toso, D. Baranov, C. Giannini, S. Marras, L. Manna, *ACS Mater. Lett.* **2019**, *1*, 272.
[28] G. Raino, M. A. Becker, M. I. Bodnarchuk, R. F. Mahrt, M. V. Kovalenko, T. Stoferle, *Nature* **2018**, *563*, 671.
[29] J. S. van der Burgt, J. J. Geuchies, B. van der Meer, H. Vanrompay, D. Zanaga, Y. Zhang, W. Albrecht, A. V. Petukhov, L. Filion, S. Bals, I. Swart, D. Vanmaekelbergh, *J. Phys. Chem. C* **2018**, *122*, 15706.
[30] M. V. Kovalenko, M. I. Bodnarchuk, *CHIMIA Int. J. Chem.* **2017**, *71*, 461.
[31] D. Baranov, S. Toso, M. Imran, L. Manna, *J. Phys. Chem. Lett.* **2019**, *10*, 655.
[32] Y. Nagaoka, K. Hills-Kimball, R. Tan, R. Li, Z. Wang, O. Chen, *Adv. Mater.* **2017**, *29*, 1606666.
[33] Y. Tong, E.-P. Yao, A. Manzi, E. Bladt, K. Wang, M. Doblinger, S. Bals, P. Muller- Buschbaum, A. S. Urban, L. Polavarapu, J. Feldmann, *Adv. Mater.* **2018**, *30*, 1801117.
[34] M. Imran, P. Ijaz, D. Baranov, L. Goldoni, U. Petralanda, Q. Akkerman, A. L. Abdelhady, M. Prato, P. Bianchini, I. Infante, L. Manna, *Nano Lett.* **2018**, *18*, 7822.
[35] K.-H. Wang, J.-N. Yang, Q.-K. Ni, H.-B. Yao, S.-H. Yu, *Langmuir* **2018**, *34*, 595.

[36] N. Yazdani, M. Jansen, D. Bozyigit, W. M. Lin, S. Volk, O. Yarema, M. Yarema, F. Juranyi, S. D. Huber, V. Wood, *Nat. Commun.* **2019**, *10*, 4236.
[37] G. Rainó, H. Utzat, M. G. Bawendi, M. V. Kovalenko, *MRS Bull.* **2020**, *45*, 841.
[38] I. Cherniukh, T. V. Sekh, G. Raino, O. J. Ashton, M. Burian, A. Travesset, M. Athanasiou, A. Manoli, R. A. John, M. Svyrydenko, V. Morad, Y. Shynkarenko, F. Montanarella, D. Naumenko, H. Amenitsch, G. Itskos, R. F. Mahrt, T. Stoferle, R. Erni, M. V. Kovalenko, M. I. Bodnarchuk, *ACS Nano* **2022**, *16*, 7210.
[39] V. S. Chirvony, S. Gonzalez-Carrero, I. Suarez, R. E. Galian, M. Sessolo, H. J. Bolink, J. P. Martinez-Pastor, J. Perez-Prieto, *J. Phys. Chem. C* **2017**, *121*, 13381.
[40] I. Afek, O. Ambar, Y. Silberberg, *Science* **2010**, *328*, 879.
[41] C. S. Muñoz, E. Del Valle, A. G. Tudela, K. Mu¨ller, S. Lichtmannecker, M. Kaniber, C. Tejedor, J. Finley, F. Laussy, *Nat. Photonics* **2014**, *8*, 550.
[42] W. P. Schleich, K. S. Ranade, C. Anton, M. Arndt, M. Aspelmeyer, M. Bayer, G. Berg, T. Calarco, H. Fuchs, E. Giacobino, M. Grassl, P. Hänggi, W. M. Heckl, I.-V. Hertel, S. Huelga, F. Jelezko, B. Keimer, J. P. Kotthaus, G. Leuchs, N. Lütkenhaus, U. Maurer, T. Pfau, M. B. Plenio, E. M. Rasel, O. Renn, C. Silberhorn, J. Schiedmayer, D. Schmitt-Landsiedel, K. Schönhammer, et al., *Appl. Phys. B* **2016**, *122*, 130.
[43] M. A. Boles, M. Engel, D. V. Talapin, *Chem. Rev.* **2016**, *116*, 11220.
[44] C. B. Murray, C. Kagan, M. Bawendi, *Annu. Rev. Mater. Sci.* **2000**, *30*, 545.
[45] J. J. Geuchies, C. Van Overbeek, W. H. Evers, B. Goris, A. De Backer, A. P. Gantapara, F. T. Rabouw, J. Hilhorst, J. L. Peters, O. Konovalov, A. V. Petukhov, M. Dijkstra, L. D. A. Siebbeles, S. van Aert, S. Bals, D. Vanmaekelbergh, *Nat. Mater.* **2016**, *15*, 1248.
[46] J. Li, X. Yuan, P. Jing, J. Li, M. Wei, J. Hua, J. Zhao, L. Tian, *RSC Adv.* **2016**, *6*, 8278311.
[47] O. H.-C. Cheng, T. Qiao, M. Sheldon, D. H. Son, *Nanoscale* **2020**, *12*, 13113.
[48] W. Shcherbakov-Wu, P. C. Sercel, F. Krieg, M. V. Kovalenko, W. A. Tisdale, *J. Phys. Chem. Lett.* **2021**, *12*, 8088.
[49] D. D. Blach, V. A. Lumsargis, D. E. Clark, C. Chuang, K. Wang, L. Dou, R. D. Schaller, J. Cao, C. W. Li, L. Huang, *Nano Lett.* **2022**, *22*, 7811.
[50] B. Zhang, L. Goldoni, C. Lambruschini, L. Moni, M. Imran, A. Pianetti, V. Pinchetti, S. Brovelli, L. De Trizio, L. Manna, *Nano Lett.* **2020**, *20*, 8847.
[51] V. S. Chirvony, K. S. Sekerbayev, H. P. Adl, I. Suarez, Y. T. Taurbayev, A. F. Gualdron- Reyes, I. Mora-Sero, J. P. Martinez-Pastor, *J. Lumin.* **2020**, *221*, 117092.
[52] Q. Han, W. Wu, W. Liu, Q. Yang, Y. Yang, *J. Lumin.* **2018**, *198*, 350.
[53] E. M. Lee, W. A. Tisdale, A. P. Willard, *J. Vac. Sci. Technol., A* **2018**, *36*, 068501.
[54] F. Mattiotti, M. Kuno, F. Borgonovi, B. Janko, G. L. Celardo, *Nano Lett.* **2020**, *20*, 7382.
[55] J. Maes, L. Balcaen, E. Drijvers, Q. Zhao, J. De Roo, A. Vantomme, F. Vanhaecke, P. Geiregat, Z. Hens, *J. Phys. Chem. Lett.* **2018**, *9*, 3093.
[56] E. Knapp, *J. Chem. Phys.* **1984**, *81*, 643.
[57] S. Davydov, *Phys.-Usp.* **1964**, *7*, 145.
[58] L. Protesescu, S. Yakunin, M. I. Bodnarchuk, F. Krieg, R. Caputo, C. H. Hendon, R. X. Yang, A. Walsh, M. V. Kovalenko, *Nano Lett.* **2015**, *15*, 3692.